LA-UR- 09-04679

Approved for public release;
distribution is unlimited.

Title:	Two-Phase Behavior and Compression Effect in the PEFC Gas Diffusion Medium
Author(s):	Partha P. Mukherjee Chao-Yang Wang Volker P. Schulz Qinjun Kang Jurgen Becker Andreas Wiegmann
Intended for:	ECS Transaction, 216th Electrochemical Society Meeting, Vienna, Austria, October 4-9, 2009

Form 836 (7/06)

Two-Phase Behavior and Compression Effect in the PEFC Gas Diffusion Medium

P. P. Mukherjee,[a] C. Y. Wang,[b] V. P. Schulz,[c] Q. Kang,[d] J. Becker,[d] and A. Wiegmann[d]

[a]Los Alamos National Laboratory, MS T003, Los Alamos, New Mexico 87545, USA

[b]Electrochemical Engine Center, Department of Mechanical & Nuclear Engineering, Pennsylvania State University, University Park, Pennsylvania 16802, USA

[c]APL-Landau GmbH, Germany

[d]Fraunhofer Institute of Industrial Mathematics (ITWM), Kaiserslautern, Germany

A key performance limitation in the polymer electrolyte fuel cell (PEFC), manifested in terms of mass transport loss, originates from liquid water transport and resulting flooding phenomena in the constituent components. A key contributor to the mass transport loss is the cathode gas diffusion layer (GDL) due to the blockage of available pore space by liquid water thus rendering hindered oxygen transport to the active reaction sites in the electrode. The GDL, therefore, plays an important role in the overall water management in the PEFC. The underlying pore-morphology and the wetting characteristics have significant influence on the flooding dynamics in the GDL. Another important factor is the role of cell compression on the GDL microstructural change and hence the underlying two-phase behavior. In this article, we present the development of a pore-scale modeling formalism coupled with realistic microstructural delineation and reduced order compression model to study the structure-wettability influence and the effect of compression on two-phase behavior in the PEFC GDL.

Introduction

In recent years, the polymer electrolyte fuel cell (PEFC) has emerged as a promising power source for a wide range of applications. Despite tremendous recent progress in enhancing the overall cell performance, a pivotal performance limitation in PEFCs centers on liquid water transport and resulting flooding in the constituent components (1). Liquid water blocks the porous pathways in the catalyst layer (CL) and gas diffusion layer (GDL) thus causing hindered oxygen transport to the reaction sites as well as covers the electrochemically active sites in the CL thereby increasing surface overpotential. This phenomenon is known as "flooding" and is perceived as the primary mechanism leading to the limiting current behavior in the cell performance. The cathode GDL plays a crucial role in the PEFC water management (1) aimed at maintaining a delicate balance between reactant transport from the gas channels and water removal from the electrochemically active sites. In the last few years, water management research has received wide attention, evidenced by the development of several macroscopic models for liquid water transport in PEFCs (2-6). The macroscopic models for liquid water transport, reported in the literature, are based on the theory of volume averaging and treat the GDL as a macrohomogeneous porous layer. Due to the macroscopic nature, the current models fail to resolve the influence of the pore morphology of the GDL on the underlying two-phase dynamics. Another important factor having strong influence on the GDL pore morphology and hence the underlying two-phase behavior is the cell clamping pressure. The importance of cell clamping pressure on fuel cell performance has been studied by several researchers. Notable works include Mathias *et al.* (7), Wilde *et al.* (8) and Ihonen *et al.* (9). Mathias *et al.* (7) reported compression and flexural behavior of carbon paper and carbon cloth GDLs and indicated the effect of compressive characteristics on the channel flow-field pressure drop. Wilde *et al.* (8) studied the impact of compression force on the GDL properties, namely electrical resistivity, pore size, and permeability for different materials and briefly described the resulting influence on PEFC performance. Ihonen and co-workers (9), on the other hand, tried to assess experimentally the influence of clamping pressure on the GDL flooding phenomena. Although substantial research, both modeling and experimental, has been conducted to study flooding and water transport in PEFCs, there is serious paucity of fundamental understanding regarding the influence of cell compression on the GDL microstructure change and the underlying two-phase behavior, which affect the cell performance.

In the current work, a comprehensive pore-scale modeling framework is presented to study the influence of cell compression and microstructure change on the flooding behavior in the PEFC non-woven carbon paper GDL.

Modeling Approach

The modeling framework comprises of three components: (1) a stochastic fibrous microstructure reconstruction model, (2) a reduced order porous media compression model, and (3) a two-phase lattice Boltzmann (LB) model for two-phase transport in the GDL microstructure.

Microstructure Reconstruction

In this work, a stochastic reconstruction technique is developed to generate non-woven carbon paper GDL microstructures. The stochastic simulation technique creates 3-D realization of the non-woven carbon paper GDL based on structural inputs, namely fiber diameter, fiber orientation and porosity which can be obtained either directly from the fabrication specifications or indirectly from the SEM (scanning electron microscope) micrographs or by experimental techniques. Details about the carbon paper GDL microstructure reconstruction method along with the underlying assumptions are elaborated in our recent work (10). Briefly, the stochastic reconstruction technique is a Poisson line process with one-parametric directional distribution where the fibers are realized as circular cylinders with a given diameter and the directional distribution provieds in-plane/through-plane anisotropy in the reconstructed GDL microstructure (10).

Figure 1 shows the reconstructed microstructure of a typical non-woven, carbon paper GDL with porosity around 72% and thickness of 180 μm along with the structural parameters in terms of the estimated pore size distribution (PSD) and the anisotropy in the in-plane vs. through-plane permeability values (10).

Reduced Order Compression Model

Detailed modeling of a porous material under compression is a challenging task of applied structural mechanics. The reduced compression model employed in the current study is based on the unidirectional morphological displacement of solid voxels in the GDL structure under load and with the assumption of negligible transverse strain. The reduced compression model is detailed in our recent work (10). However, with the reduced compression model, it is difficult to find a relation between the compression ratio

and the external load. The compression ratio is defined as the ratio of the thickness of compressed sample to that of the uncompressed sample. Nevertheless, this approach leads to reliable 3D morphology of the non-woven GDL structures under compression. Figure 2(a) shows compressed, reconstructed non-woven GDL microstructures with 20% and 40% compression along with the uncompressed structure and representative 2-D cross-sections. Due to the compression of the structure, the pore size distribution is expected to shift toward smaller pores. Figure 2(b) shows the pore size distributions of the uncompressed and 50% compressed GDL microstructures. It can be observed that the mean pore size shifts from around 17 μm to approximately 10 μm under 50% compression, while the width of the pore size distribution shows negligible variation.

Reconstructed Non-woven Carbon Paper GDL Microstructure

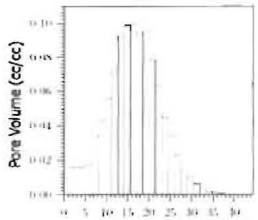

Pore Size Distribution

Permeability	In-plane	Through-plane	In-plane/Through-plane
Reconstructed GDL	30.9 darcy	21.1 darcy	1.46
Measured data	33 darcy	18 darcy	1.83

Figure 1: Reconstructed non-woven carbon paper GDL microstructure along with pore size distribution and the evaluated structural properties.

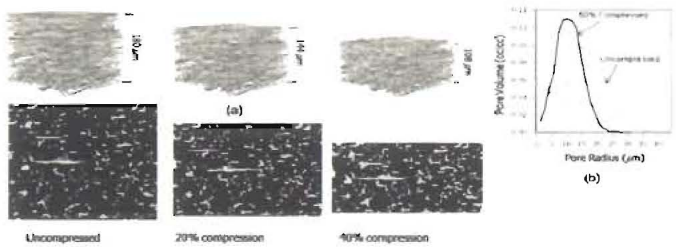

Figure 2: Reconstructed uncompressed and compressed non-woven GDL microstructures along with pore size distribution.

Two-Phase Lattice Boltzmann Model

In recent years, the lattice Boltzmann (LB) method, owing to its excellent numerical stability and constitutive versatility, has developed into a powerful technique for simulating fluid flows and is particularly successful in fluid flow applications involving interfacial dynamics and complex geometries (11). The LB method is a first-principle based numerical approach. Unlike the conventional Navier-Stokes solvers based on the discretization of the macroscopic continuum equations, lattice Boltzmann methods consider flows to be composed of a collection of pseudo-particles residing on the nodes of an underlying lattice structure which interact according to a velocity distribution function. The lattice Boltzmann method is also an ideal scale-bridging numerical scheme which incorporates simplified kinetic models to capture microscopic or mesoscopic flow physics and yet the macroscopic averaged quantities satisfy the desired macroscopic equations (11).

The two-phase lattice Boltzmann model developed in this work is based on the interaction potential model, originally proposed by Shan and Chen (12). This model introduces k distribution functions for a fluid mixture comprising of k components. Each distribution function represents a fluid component and satisfies the evolution equation. The non-local interaction between particles at neighboring lattice sites is included in the kinetics through a set of potentials. The LB equation for the kth component can be written as:

$$f_i^k(\mathbf{x}+\mathbf{e}_i\delta_t, t+\delta_t) - f_i^k(\mathbf{x},t) = -\frac{f_i^k(\mathbf{x},t) - f_i^{k(eq)}(\mathbf{x},t)}{\tau_k} \qquad [1]$$

where $f_i^k(\mathbf{x},t)$ is the number density distribution function for the kth component in the ith velocity direction at position $\mathbf{x}$ and time t, and δ_t is the time increment. In the term on the right-hand side, τ_k is the relaxation time of the kth component in lattice unit, and $f_i^{k(eq)}(\mathbf{x},t)$ is the corresponding equilibrium distribution function. The right-hand-side of Eq. [1] represents the collision term, which is simplified to the equilibrium distribution function $f_i^{k(eq)}(\mathbf{x},t)$ by the so-called BGK (Bhatnagar-Gross-Krook), or the single-time relaxation approximation (13). A three-dimensional 19-speed lattice (D3Q19, where D is the dimension and Q is the number of velocity directions), shown schematically along with the velocity directions in Fig. 3, is used in the model. Surface tension between the two phases is realized through a fluid/fluid interaction force and the wall adhesion effect i.e. the contact angle is incorporated via a fluid/solid interaction force. The details of the two-phase lattice Boltzmann model developed for this study are furnished in Ref. (12,14,15).

Two-Phase Numerical Experiment and Setup

In this study, a numerical experiment is specifically designed for investigating liquid water transport and two-phase dynamics through the reconstructed GDL microstructure. Before describing the details of the numerical experiment, it is important to mention that the two-phase transport in the PEFC GDL is characterized by capillary transport as evidenced by very low Capillary number ($Ca = \mu_2 U_2 / \sigma \sim 10^{-6}$) operation (15,16). In the Capillary number expression, U_2 and μ_2 are the non-wetting phase Darcy velocity and dynamic viscosity respectively, σ is the surface tension. In the capillary transport regime, surface forces dominate over the inertial, viscous and gravity forces (15,16).

The numerical setup is devised to simulate a *quasi-static displacement experiment*, detailed elsewhere in the literature in the context of geologic porous media transport (17),

for simulating immiscible, two-phase transport through the GDL microstructure. A non-wetting phase (NWP) reservoir is added to the porous structure at the front end and a wetting phase (WP) reservoir is added at the back end (15). It should be noted that for the *primary drainage* (PD) simulation in the hydrophobic GDL, liquid water is the NWP and air is the WP. The primary drainage process is simulated starting with zero capillary pressure, by fixing the NWP and WP reservoir pressures to be equal. Then the capillary pressure is increased incrementally by decreasing the WP reservoir pressure while maintaining the NWP reservoir pressure at the fixed initial value. The pressure gradient drives liquid water into the initially air-saturated GDL by displacing it. The details about the numerical setup corresponding to the primary drainage simulation are furnished in Refs. (15). For the subsequent two-phase simulations, a reconstructed GDL structure with $100\times100\times100$ lattice points is used keeping in mind the significant computational overhead in LB calculations. The primary objective of the quasi-static displacement simulation is to study the liquid water behavior through the fibrous GDL structure and the concurrent response to capillarity as a direct manifestation of the underlying pore-morphology

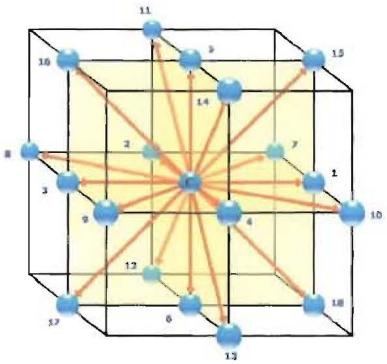

Figure 3: D3Q19 lattice structure.

Results and Discussion

Figure 4 shows the liquid water distribution as well as the invasion pattern from the *primary drainage simulation* with increasing capillary pressure in the initially air-saturated uncompressed carbon paper GDL characterized by hydrophobic wetting characteristics with a static contact angle of 140^0. Physically, this scenario corresponds to the transport of liquid water generated due to the electrochemical reaction in the CL into the otherwise air-occupied GDL in an operating fuel cell. At the initially very low capillary pressure, the invading front overcomes the barrier pressure only at some preferential locations depending upon the pore size along with the emergence of droplets owing to strong hydrophobicity. As the capillary pressure increases, several liquid water fronts start to penetrate into the air occupied domain. Further increase in capillary pressure exhibits growth of droplets at two invasion fronts, followed by the coalescence of the drops and collapsing into a single front. This newly formed front then invades into the less tortuous in-plane direction. Additionally, emergence of tiny droplets and subsequent growth can be observed in the constricted pores in the vicinity of the inlet region primarily due to strong wall adhesion forces from interactions with highly hydrophobic fibers with the increasing capillary pressure. One of the several invading fronts finally reaches the air reservoir, physically the GDL/channel interface, at a preferential location corresponding to the capillary pressure and is also referred to as the bubble point. Additionally, 2-D liquid water saturation maps on different cross-sections along the GDL through-plane direction corresponding to a representative liquid water saturation level are shown in Fig. 5 which demonstrates the porous pathways actually available for oxygen transport from the channel to the CL reaction sites. It is worth mentioning that the LB simulation is indeed able to capture the intricate liquid water dynamics including droplet interactions, flooding front formation and propagation through the hydrophobic fibrous GDL structure. Furthermore, it is important to note that the liquid water transport and flooding dyanmics through a woven carbon cloth GDL would lead to very different scenario owing to liquid water motion along individual fibers as well as between fiber bundles as opposed to that in the non-woven carbon cloth GDL. Further investigations are currently underway to understand the influence of different pore morphology and wetting characteristics of GDL structures on the resulting flooding dynamics.

Figure 6 shows the liquid water distribution as well as the invasion pattern from the *primary drainage simulation* with increasing capillary pressure in the initially air-saturated 30% compressed carbon paper GDL microstructure characterized by hydrophobic wetting characteristics with a static contact angle of 140^0, similar to its uncompressed counterpart, described earlier. The reduced compression model was used to generate the compressed structure. Similar to the uncompressed GDL, at very low initial capillary pressures, the invading front overcomes the barrier pressure only at some preferential locations depending upon the pore size. As the capillary pressure increases, several liquid water fronts start to penetrate into the air occupied domain. Owing to the compression induced microstructural change, further increase in capillary pressure exhibits coalescence of drops and concurrent merging of the fronts into a single front. This newly formed front propagates in the through-plane direction with liquid water build-up and subsequent action of capillarity. However, no preferential front migration toward the in-plane direction, as opposed to that in the uncompressed structure, is observed, which can be attributed to the increased tortuosity owing to the compression of the GDL. Emergence of droplets and subsequent growth can also be observed in the constricted pores primarily due to strong wall adhesion forces from interactions with highly hydrophobic fibers with the increasing capillary pressure. Finally, the predominant front reaches the air reservoir, physically the GDL/channel interface, at a preferential location and the corresponding capillary pressure is referred to as the bubble point. Concurrent to the bubble point, the microstructural change also reflects in the movement of water in the in-plane direction which could rather be attributed to the liquid water build-up at the corresponding saturation level, and differs significantly from the two-phase transport in the uncompressed GDL shown in Fig. 4. Additionally, the 2-D liquid water saturation maps on different cross-sections along the GDL through-plane direction corresponding to a representative liquid water saturation level are shown in Fig. 7 which demonstrates the porous pathways actually available for oxygen transport from the channel to the CL reaction sites in the compressed GDL. The roughened fiber cross-sections also suggest overlaying of fiber layers from compression leading to higher tortuosity. It is worth mentioning that the LB simulation is indeed able to capture the intricate liquid water dynamics and reflects the influence of compression induced GDL

microstructural change on the flooding behavior. Detailed investigations are currently underway to understand the influence of different pore morphology and wetting characteristics of GDL structures under the influence of compression on the resulting flooding dynamics. Furthermore, a micro-FE (finite element) formalism is also under development to capture the realistic structural mechanics effect in order to directly relate the compression load to the microstructural change of the GDL. It is important to note that the mesoscopic LB simulations provide fundamental insight into the pore-scale liquid water transport in uncompressed and compressed GDL structures and would likely enable novel GDL microstructure design for flooding mitigation.

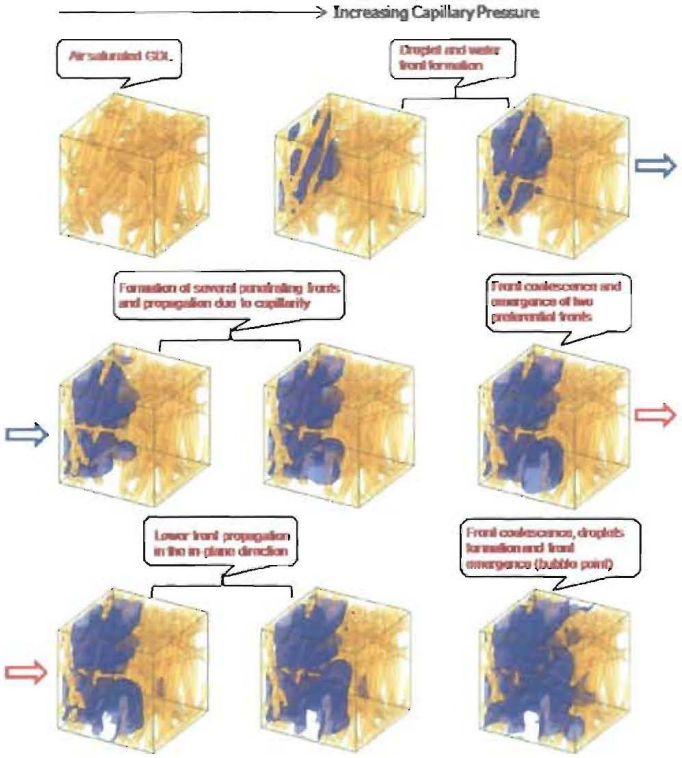

Figure 4: Advancing liquid water front with increasing capillary pressure through the initially air-saturated uncompressed GDL microstructure from the primary drainage simulation.

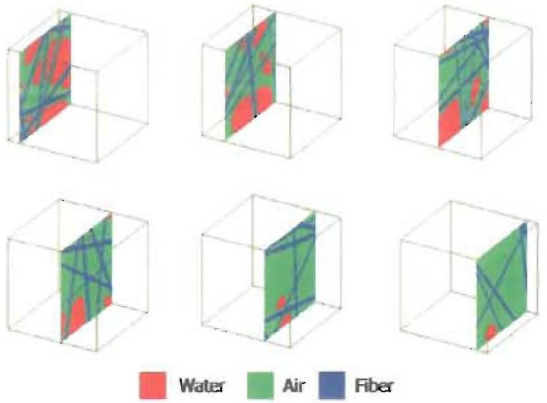

Figure 5: 2-D phase distribution maps on several cross-sections along the through-plane direction in the uncompressed GDL structure from the primary drainage simulation.

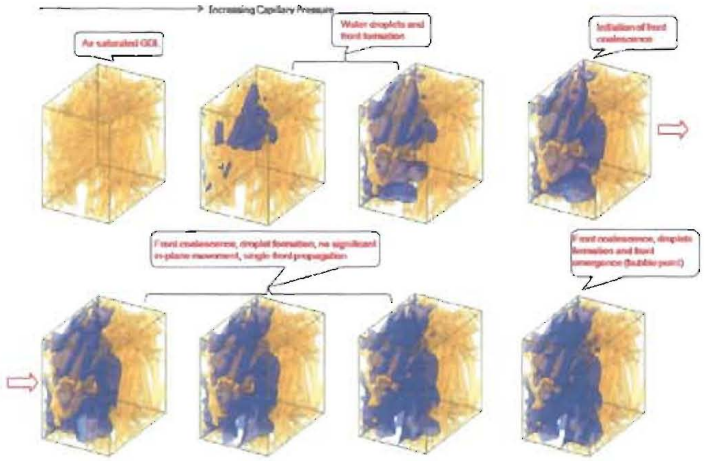

Figure 6. Advancing liquid water front with increasing capillary pressure through the initially air-saturated GDL microstructure with 30% compression from the primary drainage simulation.

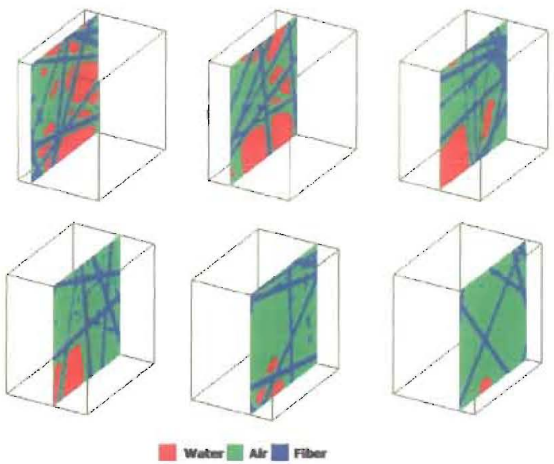

Figure 7: 2-D phase distribution maps on several cross-sections along the through-plane direction in the 30% compressed GDL structure from the primary drainage simulation

Conclusions

The gas diffusion layer plays a crucial role in the overall PEFC performance due to the transport limitation in the presence of liquid water and flooding phenomena. The cell compression affects the GDL pore morphology and hence the underlying liquid water transport characteristics. In this work, the development of a pore-scale modeling formalism including a stochastic microstructure reconstruction model, a reduced order microstructure compression model and a two-phase lattice Boltzmann model is presented in order to reveal the structure-wettability influence and the effect of compression on the underlying pore morphology and flooding dynamics in the PEFC GDL. The liquid water transport in the non-woven GDL structure with hydrophobic wetting characteristics shows intricate interfacial dynamics including droplet interactions, flooding front formation and propagation. The compressed GDL structure exhibits enhanced resistance to liquid water transport in the in-plane direction due to the change in the underlying pore morphology leading to increased tortuosity.

Acknowledgments

PPM would like to acknowledge the support of the Los Alamos National Laboratory LDRD program.

References

1. C. Y. Wang, *Chem. Rev.*, (*Washington, DC*), **104**, 4727 (2004).
2. U. Pasaogullari and C. Y. Wang, *J. Electrochem. Soc.*, **151**, 399 (2004).
3. Y. Wang and C. Y. Wang, *J. Electrochem. Soc.*, **153**, A1193 (2006).
4. A. Z. Weber and J. Newman, *J. Electrochem. Soc.*, **152**, A677 (2005).
5. J. Nam and M. Kaviany, *Int. J. Heat Mass Transfer*, **46**, 4595 (2003).
6. W. He, J. S. Yi, and T. V. Nguyen, *AIChE J.*, **46**, 2053 (2000).
7. M. F. Mathias, J. Roth, J. Fleming, and W. Lehnert, in *Handbook of Fuel Cells Fundamentals, Technology and Applications*, W. Lietsich, A. Lamm and H. A. Gasteiger, Editors, Vol 3, Ch. 42, 517, John Wiley & Sons, Chicester, 517 (2003).
8. P. M. Wilde, M. Mandel, M. Murata, and N. Berg, *Fuel Cells*, **4**, 180 (2004).
9. J. Ihonen, M. Mikkola, G. Lindbergh, *J. Electrochem. Soc.*, **151**, A1152 (2004).
10. V. P. Schulz, J. Becker, A. Wiegmann, P. P. Mukherjee, and C. Y. Wang, *J. Electrochem. Soc.*, **154**, B419 (2007).
11. S. Chen and G. D. Doolen, *Ann. Rev. Fluid Mech.*, **30**, 329 (1998).
12. X. Shan and H. Chen, *Phys. Rev. E*, **47**, 1815, 1993.
13. P. Bhatnagar, E. Gross, and M. Krook, *Phys. Rev.*, **94**, 511 (1954).
14. Q. Kang, D. Zhang, and S. Chen, *J. Fluid Mech.*, **545**, 41 (2005).
15. P. P. Mukherjee, *PhD Dissertation*, Pennsylvania State University, University Park, PA, USA (2007).
16. P. K. Sinha, P. P. Mukherjee, and C. Y. Wang, *J. Mater. Chem.*, 17, 3089 (2007).
17. J. Bear, *Dynamics of Fluids in Porous Media*, Dover, New York (1972).